Construction and Building Materials 24 (2010) 585–595

Contents lists available at ScienceDirect

Construction and Building Materials

journal homepage: www.elsevier.com/locate/conbuildmat

Axial capacity of rectangular concrete-filled steel tube columns – DOE approach

Manojkumar V. Chitawadagi [a,*], Mattur C. Narasimhan [a,1], S.M. Kulkarni [b,2]

[a] Department of Civil Engineering, National Institute of Technology Karnataka, Surathkal, Mangalore 575 025, India
[b] Department of Mechanical Engineering, National Institute of Technology Karnataka, Surathkal, Mangalore 575 025, India

ARTICLE INFO

Article history:
Received 20 January 2009
Received in revised form 12 September 2009
Accepted 12 September 2009
Available online 12 October 2009

Keywords:
Concrete-filled steel tubes
Columns
Rectangular steel tubes
Ultimate axial load
Axial shortening

ABSTRACT

This paper presents the effect of change in wall thickness of the steel tube (t), strength of in-filled concrete (f_{cu}), cross-sectional area of the steel tube (A) and length of the tube (L) on ultimate axial load and axial shortening at ultimate point of rectangular concrete-filled steel tubes (CFT). Taguchi's approach with an L9 orthogonal array is used to reduce the number of experiments. With the help of initial experiments, linear regression models are developed to predict the ultimate axial load and the axial shortening at ultimate point. A total of 243 rectangular CFT samples are tested to verify the accuracy of these models at three factors with three levels. The experimental results are analyzed using Analysis Of Variance to investigate the most influencing factor on strength and axial shortening of CFT samples. Comparisons are made with predicted column strengths using the existing design codes, AISC–LRFD-1994 and EC4-1994.

1. Introduction

The use of concrete-filled steel tubular (CFT) columns for the construction of high-rise buildings, bridges, barriers, etc. has become increasingly popular in recent years. These columns have demonstrated higher axial load capacity, better ductility performance, larger energy absorption capacity and lower strength degradation than conventional reinforced concrete and steel hollow section columns [1]. The enhancement of structural properties of CFT columns is mainly due to the composite action of steel hollow section and core concrete. The confining effect by the steel hollow section causes the core concrete to behave in a triaxial stress state while the core concrete prevents the wall of the steel hollow section from buckling inward [2].

Although CFT columns are suitable for tall buildings in high seismic regions, their use has been limited due to a lack of information about the true strength and the inelastic behavior of CFT members. There is a discrepancy in the analytical models proposed by different researchers for evaluating the strength of a CFT column and the effect of confinement [3].

Tao et al. [4] mentioned from earlier studies on CFT columns that the behavior of rectangular CFT columns differs from that of circular and square CFT columns owing to the confinement of core concrete by steel hollow section. It is shown that the performance of a concrete-filled square or rectangular steel tube is not as good as its circular counterpart. This is due to the fact that a square or rectangular steel tube cannot provide as much confining pressure to the concrete core, and that local buckling is more likely to occur. With a large aspect ratio of section, the maximum axial strength of stub columns is even less than the combination of the steel and concrete components due to the effects of local buckling.

According to past study on the concentric compression behavior of CFT columns, the ultimate axial strength of CFT columns is considerably affected by the wall thickness of the steel tube, strength of in-filled concrete and length of the CFT. The present work is intended to study the parameters affecting the ultimate axial load carrying capacity and corresponding axial shortening of the CFT using Design Of Experiments (DOE) approach. The prime factors considered to affect ultimate axial load and corresponding axial shortening under axial compression are cross-sectional area (A), wall thickness of the steel tube (t), strength of in-filled concrete (f_{cu}) and length of the CFT (L). To study the effect of slenderness ratio on ultimate load carrying capacity of the CFT, three lengths namely 1 m, 0.7 m and 0.5 m are considered. Length to width ratio (L/H) for the samples selected is 6.25–20 and width to thickness of the steel tube (B/t) ratio is 9.4–25. For each length of the CFT column, samples tested are 81 (Table 1), consisting of three cross-sectional areas, three wall thicknesses and three grades of in-filled concrete ($3^3 = 27$). For each combination of CFT, three samples are tested and average value is considered. A total of 243 experiments are conducted to determine the effect of these four factors

* Corresponding author. Tel.: +91 824 247000 3041; mobile: +91 9449837148.
E-mail addresses: manojkumar1966@gmail.com, mvc@bvb.edu (M.V. Chitawadagi), mattur_cn@yahoo.com (M.C. Narasimhan), samakoo@yahoo.com (S.M. Kulkarni).
[1] Tel.: +91 824 247000 3041; mobile: +91 9449163427.
[2] Tel.: +91 824 247000 3656; mobile: +91 9449086656.

0950-0618/$ - see front matter © 2009 Elsevier Ltd. All rights reserved.
doi:10.1016/j.conbuildmat.2009.09.006

Nomenclature

A	cross-sectional area of the steel tube	P_{ue}	measured ultimate axial load
B	width of the steel tube	t	wall thickness of the steel tube
H	depth of the steel tube	$\delta_{uc\text{-}N}$	predicted axial shortening at ultimate load based on initial nine experiments
f_{cu}	cube compressive strength of concrete at 28 days	$\delta_{uc\text{-}R}$	predicted axial shortening at ultimate load based on Response Surface Method
$P_{uc\text{-}N}$	predicted ultimate axial load based on initial nine experiments	δ_{ue}	measured axial shortening at ultimate point
$P_{uc\text{-}R}$	predicted ultimate axial load based on Response Surface Method		
$P_{uc\text{-}27}$	predicted ultimate axial load based on 27 experiments		

on responses namely ultimate axial load (P_{ue}) and axial shortening at ultimate point (δ_{ue}).

2. Experimental programme

In the present investigation CFTs with three different cross-sectional areas each with three different wall thicknesses are selected (B/t = 9.4–25). Factors and levels considered for each length of the CFT is shown in Table 2. Three different grades concrete mixes of M_{30}, M_{40} and M_{50} are considered as candidate mixes. Design mixes are prepared using locally available Portland Pozzolana Cement (PPC), crushed granite jelly (12.0 mm down) and river sand. Mix designs of these three grades of concrete are made based on the guidelines of IS 10262-1982 [5]. The mix proportions adopted for the three grades are shown in Table 3. In order to ensure proper compaction, higher degree of workability, i.e. 80–100 mm slump is adopted for the concrete mixes. This is achieved by using silica fume and super plasticizer as admixtures. Standard cubes (100 mm size) are tested to determine the compressive strength of the concrete mixes at 28 days.

Cold-formed, mild steel tubes, with yield strength of 250 MPa and 1000 mm, 700 mm and 500 mm in length are used in the present investigation. These tubes are seam welded. The edges of the tubes are finished. Outer surface of the steel tubes are painted to avoid the corrosion. The insides of the tubes are wire brushed and the deposits of grease and oil, if any, are removed. The allowable D/t ratios of the steel hollow sections are less than the limits specified in EC4-1994 [6] and thus the premature buckling failure of CFT specimens is avoided.

While placing the concrete steel tubes are kept in upright position in the stand specially prepared. Bottom end of the steel tube is covered with polythene sheet tightly and concrete is poured from the top. Concrete is filled in the steel tube in approximately four equal layers and each layer is well compacted. Top of the concrete is trimmed off using a trowel and steel tube is kept undisturbed until it is taken out from the stand after 24 h to keep in water for curing.

3. Test setup and procedure

The column specimens are tested at 28 days of age. The tests are conducted in a 1000 kN capacity Column Testing Machine (Fig. 1). Linearly Varying Displacement Transducers (LVDT) are placed at one fourth, at mid-height and at three fourth heights of the sample to measure lateral deformation. Prior to the actual tests, a pre-load of approximately 2–5 kN is applied so that the platens of the testing machine are firmly attached to both ends of the specimen. The axial load is then applied slowly by careful manipulation of the loading-valves. The readings of the applied load, axial shortening and LVDT readings are recorded at appropriate load increments.

4. Results and discussion

4.1. Design Of Experiments approach

In order to save time and material cost involved in experimentation, lesser number of experiments is desired. Therefore, the Taguchi method [7] was introduced as a useful engineering methodology to find proper combination of structural parameters and to analyze with minimum number of experiments. Therefore nine experiments are carried out according to combination levels indicted by an L9 orthogonal array (Table 4) for each length of the CFT sample. An orthogonal array helps in determining minimum number of trials that are necessary, and the factor levels for each parameter in each trial. A general L9 orthogonal array consists of combination of experiments to carry with three factors each at three levels. For each sample three replicas were tested.

4.2. Main effect plots and Analysis Of Variance

After performing experiments as per Taguchi's experimental design, main effect plots for ultimate axial load and axial shortening at ultimate load are plotted for 1 m, 0.7 m and 0.5 m length of the CFTs. A main effect is the direct effect of parameters on

Table 1
Details of CFT samples tested for each 1 m, 0.7 m and 0.5 m length of the column.

Sl. No.	Notation	No. of samples	Notation	No. of samples	Notation	No. of samples
1	$A_1t_1M_{30}$	3	$A_2t_1M_{30}$	3	$A_3t_1M_{30}$	3
2	$A_1t_2M_{30}$	3	$A_2t_2M_{30}$	3	$A_3t_2M_{30}$	3
3	$A_1t_3M_{30}$	3	$A_2t_3M_{30}$	3	$A_3t_3M_{30}$	3
4	$A_1t_1M_{40}$	3	$A_2t_1M_{40}$	3	$A_3t_1M_{40}$	3
5	$A_1t_2M_{40}$	3	$A_2t_2M_{40}$	3	$A_3t_2M_{40}$	3
6	$A_1t_3M_{40}$	3	$A_2t_3M_{40}$	3	$A_3t_3M_{40}$	3
7	$A_1t_1M_{50}$	3	$A_2t_1M_{50}$	3	$A_3t_1M_{50}$	3
8	$A_1t_2M_{50}$	3	$A_2t_2M_{50}$	3	$A_3t_2M_{50}$	3
9	$A_1t_3M_{50}$	3	$A_2t_3M_{50}$	3	$A_3t_3M_{50}$	3
No. of samples	A_1 series	27	A_2 series	27	A_3 series	27
Total no. of CFT samples tested for each length					27 + 27 + 27 = 81	

Note:
M_{30} = Concrete mix of characteristic strength of 30 N/mm^2 with cube strength at 28 days is 41.6 N/mm^2.
M_{40} = Concrete mix of characteristic strength of 40 N/mm^2 with cube strength at 28 days is 51.2 N/mm^2.
M_{50} = Concrete mix of characteristic strength of 50 N/mm^2 with cube strength at 28 days is 60.6 N/mm^2.
Axial load and axial shortening are the values of average of three samples. For each length of CFT 81/3 = 27 experimental values for axial load and axial shortening are taken.

Table 2
Factors and levels selected for each length of the CFT column.

Levels	Factors		
	Size and area of the steel tube (mm^2)	Wall thickness of the steel tube (mm)	Strength of in-filled concrete (N/mm^2)
Level-1	[25 × 50] 1250 (A_1)	1.6 (t_1)	41.6 (M_{30})
Level-2	[40 × 60] 2400 (A_2)	2.0 (t_2)	51.2 (M_{40})
Level-3	[40 × 80] 3200 (A_3)	2.65 (t_3)	60.6 (M_{50})

response or dependent variable. Typical main effect plots of parameters with respect to ultimate axial load and associated axial shortening for CFTs of 1 m and 0.5 m long are shown in Figs. 2–7. It is plotted by considering means of responses at each level of the parameters, as shown in Tables 5 and 6. It can be noted that increase in cross-sectional area, wall thickness and strength of concrete will increase the ultimate axial load capacity for 1 m, 0.7 m and 0.5 m length of CFTs. But cross-sectional area of the steel tube has the most significant effect on both the ultimate axial load capacity and corresponding axial shortening of all the three lengths of the CFTs. Strength of in-fill concrete and the wall thickness of the CFT have respectively lesser effects compared to cross-sectional area of the steel tube. Next to cross-sectional area wall thickness has most influenced on ultimate axial load carrying capacity of CFTs. Increase in wall thickness, helps to postpone the local buckling failure. Increase in strength of in-filled concrete has more effect than the wall thickness when axial shortening of the CFTs are concerned. To assess the rank of each of the parameter, the deltas of the means of each level of all the factors are calculated and shown in Tables 5 and 6. The delta means the value of the maximum mean minus the minimum one. Most influencing factor ranks first.

The experimental results are also analyzed using Analysis Of Variance (ANOVA) technique. ANOVA is statistical analysis and diagnostic tool, which helps to reduce the error variance and quantifies the dominance of a control factor. This analysis aids in justifying the effects of input changes on the responses in an experiment. From ANOVA it is found that, cross-sectional area of the steel tube has the most significant effect on both the ultimate axial load carrying capacity and associated axial shortening for all

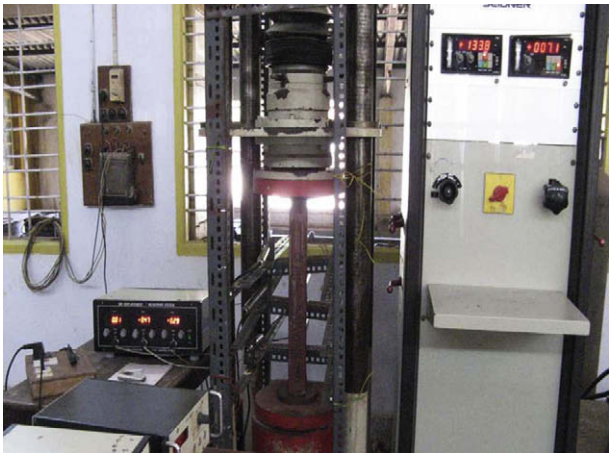

Fig. 1. Compression test on CFT sample in the Column Testing Machine – an experimental setup.

lengths of the CFTs, while the strength of in-fill concrete and the wall thickness have respectively lesser influence on these responses. Greater F value confirms that cross-sectional area of the steel tube has a most influential effect among all factors on responses of CFTs of all the three lengths. Typical ANOVA details for CFTs of 1 m length are shown in Tables 7 and 8.

4.3. Verification of Taguchi's method for CFTs

After conducting the initial nine experiments, linear regression models are developed (Eqs. (1)–(6)) to predict ultimate axial load and axial shortening at ultimate point for each length of the CFT samples.

CFTs – 1 m long

$$P_{\text{uc-N}} = -192 + 0.086A + 36.9t + 1.80f_{\text{cu}} \quad (1)$$

$$\delta_{\text{uc-N}} = 2.25 + 1.28 \times 10^{-3}A + 0.177t - 0.0235f_{\text{cu}} \quad (2)$$

Table 3
Concrete mix proportions.

Sl. No	Mix designation	Binder (B) (kg/Cub m)		Proportions B:FA:CA	W/B ratio	Super plasticizer % (by wt. of binder)	28 days compressive strength (f_{cu}) (N/mm^2)	Slump (mm)
		Cement	Silica fume					
1	M_{30}	390	20	1:1.80:2.28	0.45	2.0	41.6	90
2	M_{40}	410	20	1:1.76:2.16	0.40	2.2	51.2	80
3	M_{50}	430	20	1:1.67:2.04	0.38	2.6	60.6	80

Table 4
L9 orthogonal array adopted and experimental results – for each length of CFT.

Notation	Ultimate axial load P_{ue} (kN)			Axial shortening at ultimate point δ_{ue} (mm)		
	1 m	0.7 m	0.5 m	1 m	0.7 m	0.5 m
$A_1t_1M_{30}$	41.6	83.3	99.6	3.4	3.6	4.0
$A_1t_2M_{40}$	68.7	112.7	119.6	2.6	3.3	3.7
$A_1t_3M_{50}$	105.1	142.0	151.8	3.1	3.4	4.0
$A_2t_1M_{40}$	163.1	181.2	188.1	4.2	4.5	4.6
$A_2t_2M_{50}$	195.0	208.7	218.0	4.6	4.2	4.1
$A_2t_3M_{30}$	187.0	212.0	220.0	4.7	5.1	5.7
$A_3t_1M_{50}$	228.1	246.8	255.0	5.1	4.7	5.5
$A_3t_2M_{30}$	197.5	244.0	251.7	6.0	5.5	6.1
$A_3t_3M_{40}$	254.5	273.4	277.0	5.5	5.2	6.0

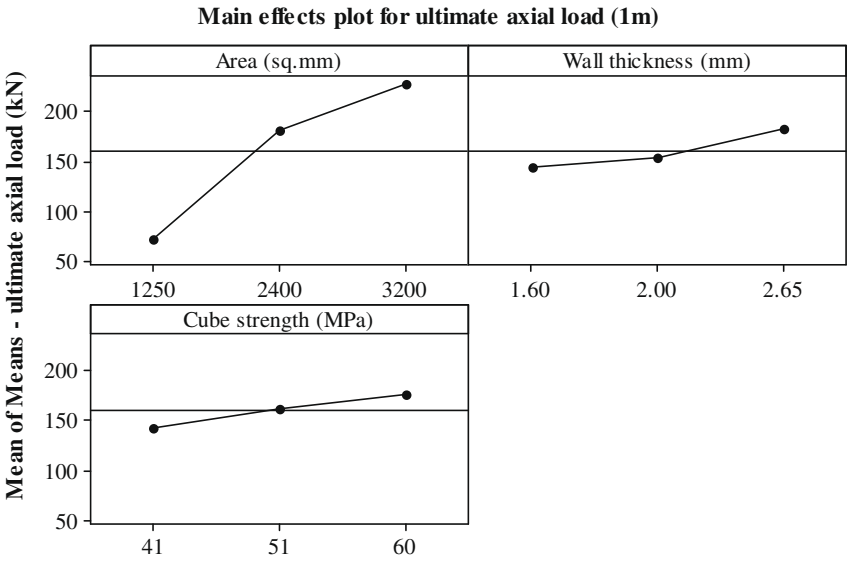

Fig. 2. Main effects plot for axial load at ultimate point for CFTs of 1 m long.

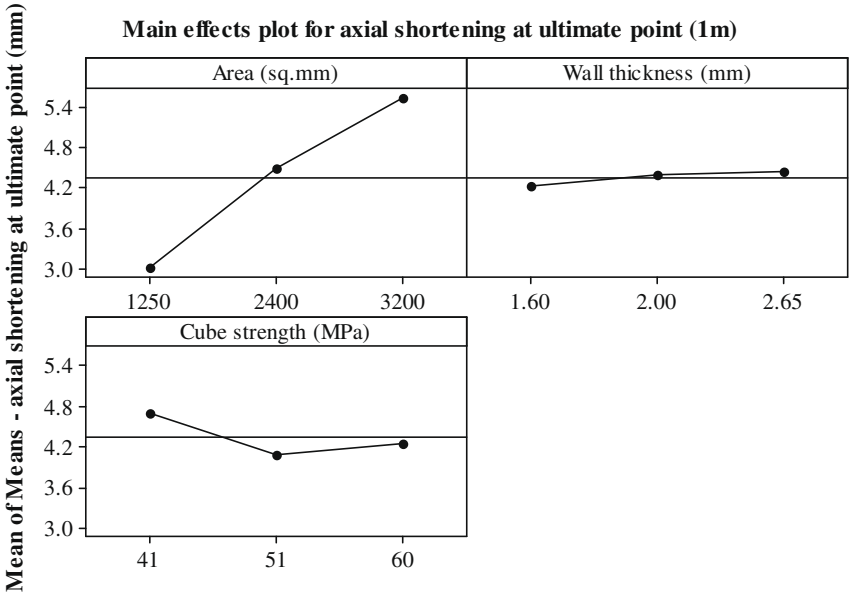

Fig. 3. Main effects plot for axial shortening at ultimate load for CFTs of 1 m long.

CFTs – 0.7 m long

$$P_{\text{uc-N}} = -105 + 0.0731A + 36.4t + 1.02f_{\text{cu}} \quad (3)$$

$$\delta_{\text{uc-N}} = 3.46 + 8.2 \times 10^{-4}A + 0.293t - 0.0335f_{\text{cu}} \quad (4)$$

CFTs – 0.5 m long

$$P_{\text{uc-N}} = -80.4 + 0.0708A + 33.4t + 0.930f_{\text{cu}} \quad (5)$$

$$\delta_{\text{uc-N}} = 3.41 + 9.93 \times 10^{-4}A + 0.548t - 0.0388f_{\text{cu}} \quad (6)$$

$P_{\text{uc-N}}$ is the predicted ultimate axial load based on initial nine experiments (kN), $\delta_{\text{uc-N}}$ is the predicted axial shortening at ultimate load based on initial nine experiments (mm), A is the cross-sectional area of the steel tube (mm^2), t is the wall thickness of the steel tube (mm), and f_{cu} is the cube compressive strength of concrete at 28 days (MPa).

These models are used to predict the axial load carrying capacity and associated axial shortening at ultimate point of the all other CFT samples used in the experimental programme. To verify the accuracy of such predictions of the load carrying capacity and corresponding axial shortening, actual axial compression tests are now conducted for remaining samples, and a comparison of experimental values is made with the predicted values. It is observed that the regression models based on nine experiments predict the axial load carrying capacity at ultimate point, very well but reasonably well for axial shortening at ultimate point for all the three lengths of the CFTs. A plot of experimental values vs. predicted ($P_{\text{uc-N}}$ vs. P_{ue} and $\delta_{\text{uc-N}}$ vs. δ_{ue}) values for each 1 m, 0.7 m and 0.5 m length of the CFTs are shown in Figs. 8–10.

Using the results of all the 27 experiments conducted for each length of the CFTs, a simple linear regression models are also developed. Such a linear regression model for 0.5 m length of the CFTs is shown in Eq. (7). Further to validate this model, part of

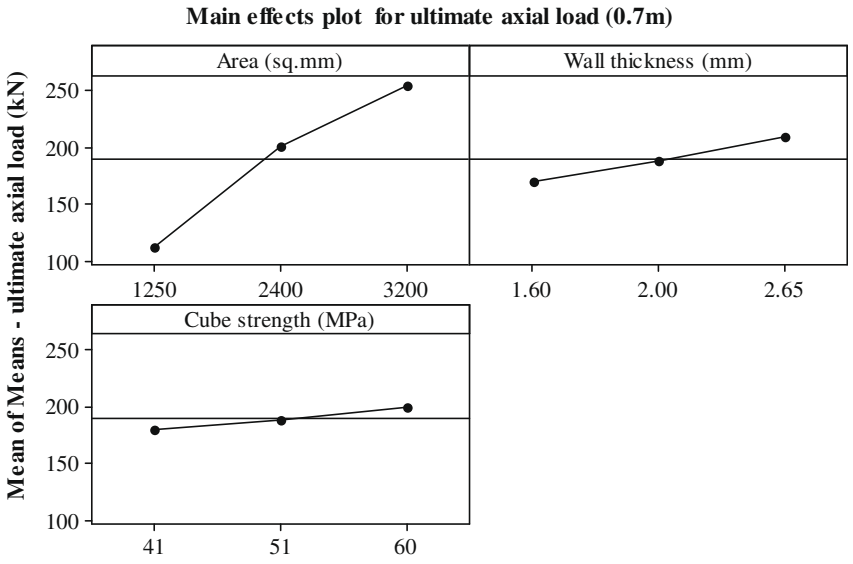

Fig. 4. Main effects plot for axial load at ultimate point for CFTs of 0.7 m long.

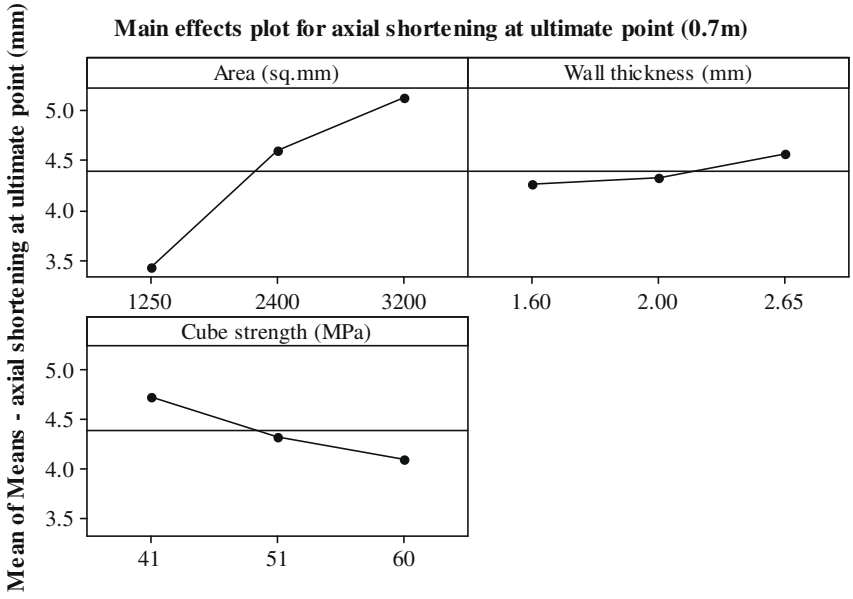

Fig. 5. Main effects plot for axial shortening at ultimate load for CFTs of 0.7 m long.

the experimental test results of Han [8], Shakir-Khaleel and Zegghiche [9], Shakir-Khaleel and Mouli [10] and Schneider [11] are used and axial compressive strengths of those CFTs were predicted using Eq. (7). It is found that the regression model predicts the axial load carrying capacities of the CFTs, very well. A plot of experimental values vs. predicted values based on Eq. (7) is shown in Fig. 11.

$$P_{\text{uc-27}} = -94.7 + 0.0728A + 33.8t + 1.08f_{\text{cu}} \quad (7)$$

$P_{\text{uc-27}}$ is the generalized linear regression model for 0.5 m CFTs based on 27 experiments (kN)

4.4. Interaction models

Based on the test results of these 27 experiments performed for each length of the CFTs, regression models are developed (Eqs. (8)–(13)) using Response Surface Method (RSM), to account the interaction between the test variables on ultimate axial load carrying capacity and corresponding axial shortening.

CFTs – 1 m long

$$P_{\text{uc-R}} = (-342.076) + (13.58A) + (78.624t) + (4.247f_{\text{cu}}) - (0.17A^2) - (8.48t^2) - (0.026f_{\text{cu}}^2) + (0.427A \cdot t) + (0.023A \cdot f_{\text{cu}}) - (0.267t \cdot f_{\text{cu}}) \quad (8)$$

$$\delta_{\text{uc-R}} = 8.6443 + (0.1103A) - (1.0832t) - (0.213f_{\text{cu}}) + (0.0006A^2) + (0.1444t^2) + (0.0013f_{\text{cu}}^2) - (0.0106A \cdot t) + (0.00042A \cdot f_{\text{cu}}) + (0.0186t \cdot f_{\text{cu}}) \quad (9)$$

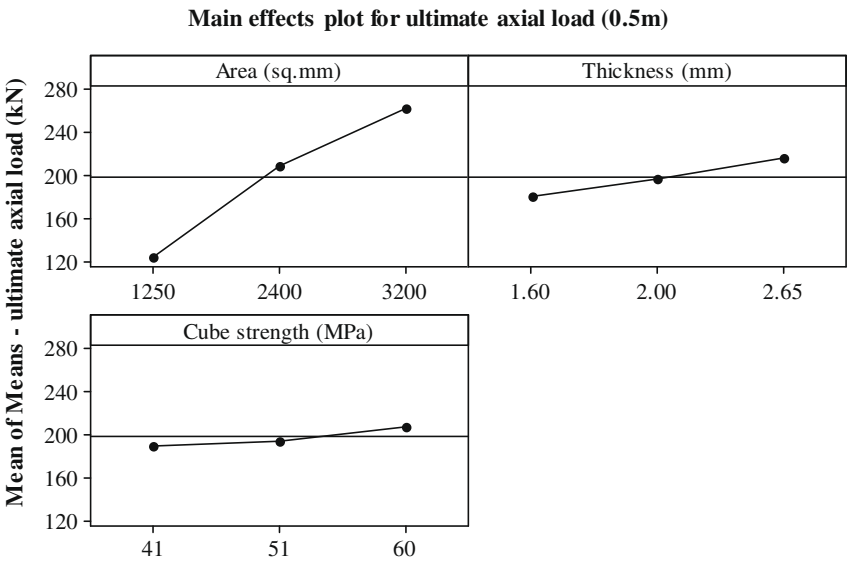

Fig. 6. Main effects plot for axial load at ultimate point for CFTs of 0.5 m long.

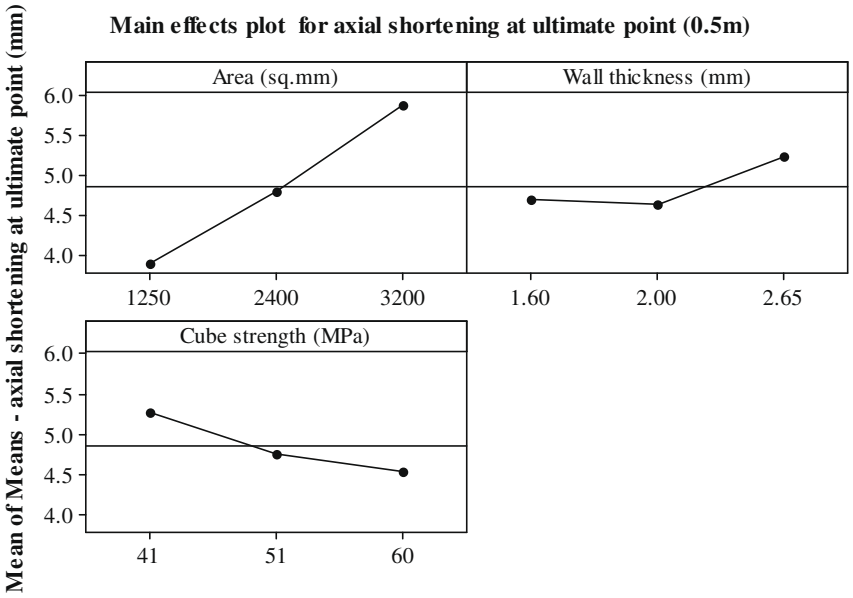

Fig. 7. Main effects plot for axial shortening at ultimate load for CFTs of 0.5 m long.

Table 5
Response table for means of mean values of each level – ultimate axial load.

Level	Length of the CFT – 1.0 m			Length of the CFT – 0.7 m			Length of the CFT – 0.5 m		
	A (mm^2)	t (mm)	f_{cu} (N/mm^2)	A (mm^2)	t (mm)	f_{cu} (N/mm^2)	A (mm^2)	t (mm)	f_{cu} (N/mm^2)
1	71.80	144.27	142.03	112.7	170.4	179.8	123.7	180.9	190.4
2	181.70	153.73	162.10	200.6	188.5	189.0	208.7	196.4	194.9
3	226.70	182.20	176.07	254.7	209.1	199.2	261.2	216.3	208.3
Delta	154.90	37.93	34.03	142.1	38.8	19.4	137.6	35.4	17.8
Rank	1	2	3	1	2	3	1	2	3

CFTs – 0.7 m long

$$P_{uc\text{-}R} = (-229.993) + (10.45A) - (111.376t) - (1.637f_{cu}) + (0.049A^2) - (17.306t^2) - (0.004f_{cu}^2) - (0.171A \cdot t) - (0.011A \cdot f_{cu}) + (0.025t \cdot f_{cu}) \quad (10)$$

$$\delta_{uc\text{-}R} = (4.2609) + (0.1672A) + (0.2378t) - (0.1036f_{cu}) - (0.0021A^2) - (0.0325t^2) + (0.0005f_{cu}^2) - (0.00013A \cdot t) + (0.0004A \cdot f_{cu}) + (0.0064t \cdot f_{cu}) \quad (11)$$

Table 6
Response table for means of mean values of each level of three factors – axial shortening at ultimate point.

Level	Length of the CFT – 1.0 m			Length of the CFT – 0.7 m			Length of the CFT – 0.5 m		
	A (mm^2)	t (mm)	f_{cu} (N/mm^2)	A (mm^2)	t (mm)	f_{cu} (N/mm^2)	A (mm^2)	t (mm)	f_{cu} (N/mm^2)
1	3.03	4.23	4.70	3.43	4.26	4.73	3.90	4.70	5.26
2	4.50	4.40	4.10	4.60	4.33	4.33	4.80	4.63	4.76
3	5.53	4.43	4.26	5.13	4.56	4.10	5.86	5.23	4.53
Delta	2.50	0.20	0.60	1.70	0.30	0.63	1.96	0.60	0.73
Rank	1	3	2	1	3	2	1	3	2

Table 7
ANOVA table for the response – axial load at ultimate point – 1 m.

Source	DF	Sum of squares	Adj. MS	F
Area	2	3809.7	19048.5	334.16
Thickness	2	2338.9	1169.5	20.52
Cube strength of the concrete	2	1756.0	878.0	15.40
Error	2	114.0	57.0	
Total	8	42305.9		

Table 8
ANOVA table for the response – axial shortening at ultimate point – 1 m.

Source	DF	Sum of squares	Adj. MS	F
Area	2	9.468	4.734	41.37
Thickness	2	0.068	0.034	0.30
Cube strength of the concrete	2	0.575	0.287	2.51
Error	2	0.228	0.114	
Total	8	10.34		

CFTs – 0.5 m long

$$P_{uc\text{-}R} = (-193.25) + (9.745A) + (69.877t) + (2.535f_{cu}) - (0.031A^2) - (9.178t^2) - (0.012f_{cu}^2) - (0.08A \cdot t) - (0.019A \cdot f_{cu}) + (0.102t \cdot f_{cu}) \quad (12)$$

$$\delta_{uc\text{-}R} = (2.7834) + (0.0021A) + (2.4680t) - (0.0517f_{cu}) - (0.0029A^2) - (0.2706t^2) + (0.00006f_{cu}^2) - (0.0249A \cdot t) + (0.0004A \cdot f_{cu}) + (0.0045t \cdot f_{cu}) \quad (13)$$

$P_{uc\text{-}R}$ is the predicted ultimate axial load based on Response Surface Method (kN), $\delta_{uc\text{-}R}$ is the predicted axial shortening at ultimate load based on Response Surface Method (mm), A is the cross-sectional area of the steel tube (cm^2), t is the wall thickness of the steel tube (mm), and f_{cu} is the cube compressive strength of concrete at 28 days (MPa).

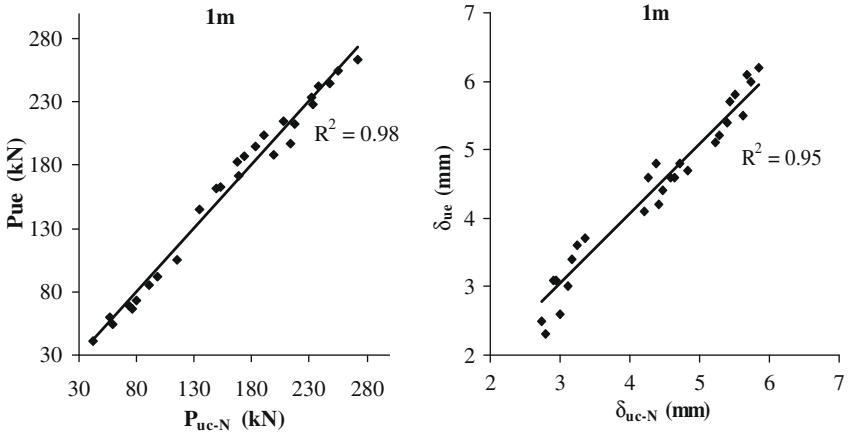

Fig. 8. Predicted values of axial load and axial shortening at ultimate point vs. experimental results – linear regression analysis (1 m).

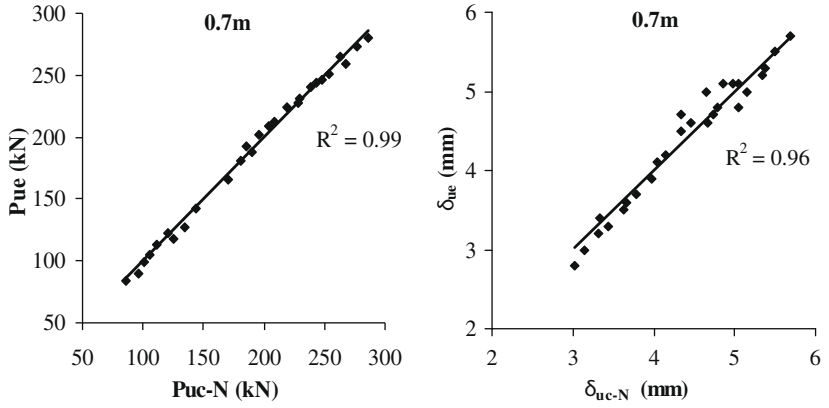

Fig. 9. Predicted values of axial load and axial shortening at ultimate point vs. experimental results – linear regression analysis (0.7 m).

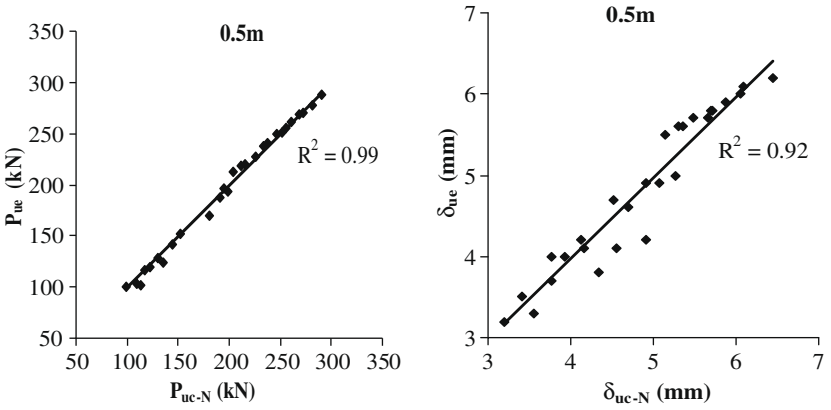

Fig. 10. Predicted values of axial load and axial shortening at ultimate point vs. experimental results – linear regression analysis (0.5 m).

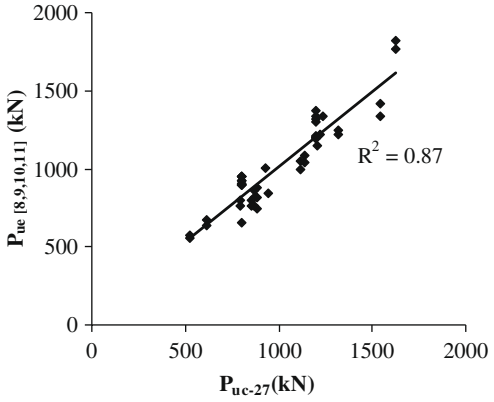

Fig. 11. Comparison between predicted column strengths using generalized regression model and test results [8–11].

Using these regression models, ultimate axial load and corresponding axial shortening of CFTs are predicted. A plot of actual experimental values vs. predicted values for each 1 m, 0.7 m and 0.5 m length of the CFTs are shown in Figs. 12–14. It is found that these interactions are more accurate for prediction of ultimate axial load as compared to axial shortening at ultimate point for all the three lengths of the CFTs.

4.5. Interaction plots

Response surface plots and Contours plots for axial load for each 1 m, 0.7 m and 0.5 m length of CFTs have been drawn using MINITAB (version 14). Response surface plots indicate the effect of any two variables together on the axial load capacity at ultimate point. A typical response surface plot shown in Fig. 15 explains the effect of wall thickness and cube strength of in-fill concrete together on the axial load capacity at ultimate point. Contour plots are useful, to arrive at proper combination of tube cross-sectional area, wall thickness and cube strength of in-fill concrete for the given values of axial load or axial shortening at ultimate point of CFTs. Typical contour plots for axial load of 0.7 m long CFTs is shown in Fig. 16. Overlaid contour plots are useful to choose combination of any two of the variables amongst cross-sectional area, wall thickness and cube strength of in-filled concrete for a certain range of design axial load capacity and corresponding axial shortening. A typical overlaid contour plots are shown in Figs. 17 and 18. Fig. 17 demonstrates the combination of cube strength of in-fill concrete and wall thickness for the ultimate axial load capacity of the range 220–240 kN and corresponding axial shortening of the range 5.5–5.7 mm for the CFT of 1 m long. Similarly Fig. 18 shows combination of cube strength of in-fill concrete and wall thickness for the axial load capacity of the range 260–280 kN, and corresponding axial shortening of the range 5.8–6.0 mm for the CFTs of 0.5 m long.

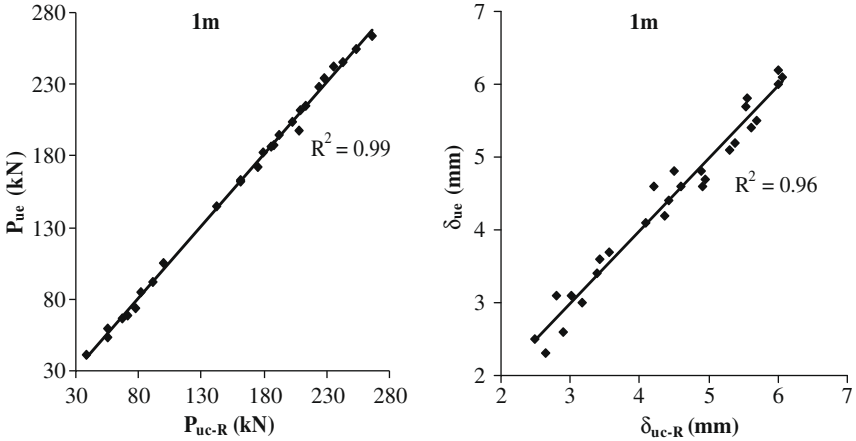

Fig. 12. Predicted values of axial load and axial shortening at ultimate point vs. experimental results – regression analysis based on RSM (1.0 m).

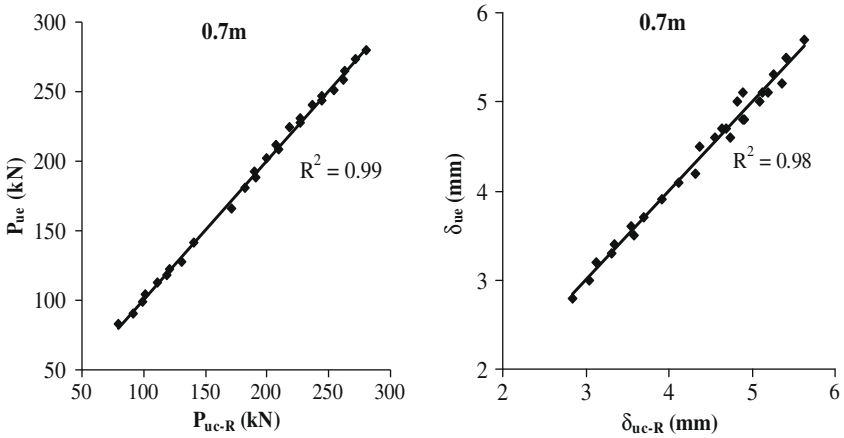

Fig. 13. Predicted values of axial load and axial shortening at ultimate point vs. experimental results – regression analysis based on RSM (0.7 m).

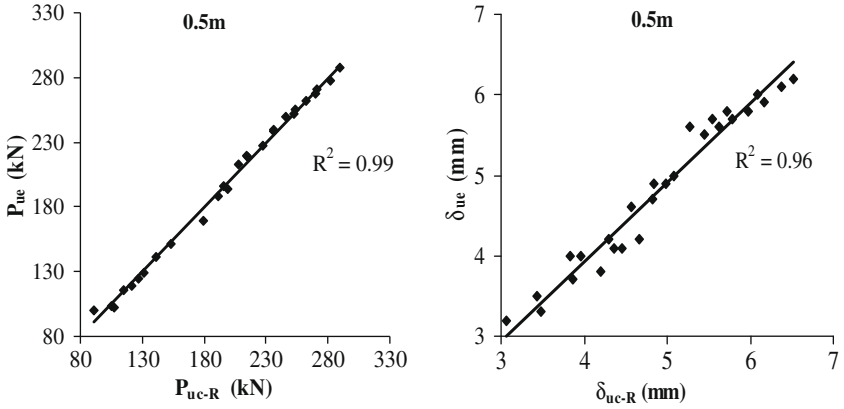

Fig. 14. Predicted values of axial load and axial shortening at ultimate point vs. experimental results – regression analysis based on RSM (0.5 m).

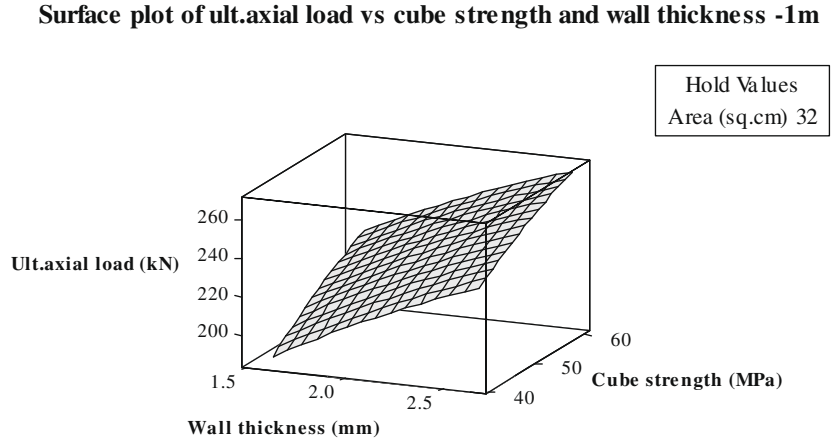

Fig. 15. Surface plot of axial load at ultimate point vs. cube strength and wall thickness for CFTs – 1 m long.

4.6. Comparison of experimental results with AISC–LRFD and EC4 specifications

The results obtained in the present experimental work were compared with the predictions based on EC4-1994 [6] and AISC-LRFD-1994 [12] code provisions. EC4 uses limit state concept to achieve the aims of serviceability and safety by applying partial safety factor to load and material properties. While calculating predicted values from design codes, all the partial safety factors are taken as unity. Comparisons of the experimental ultimate load of test specimens with predictions based on design code provisions for three lengths of CFTs are shown in

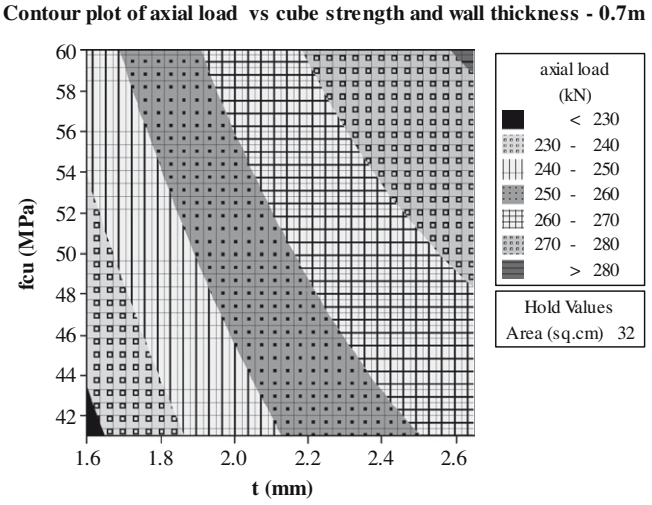

Fig. 16. Contour plot of axial load at ultimate point vs. and cube strength and wall thickness for CFTs –0.7 m long.

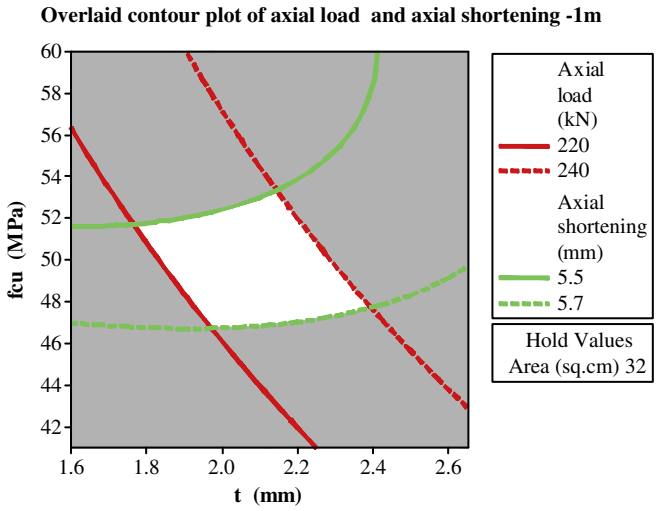

Fig. 17. Overlaid contour plot of axial load and axial shortening at ultimate point for CFTs – 1 m long (A = 3200 mm^2).

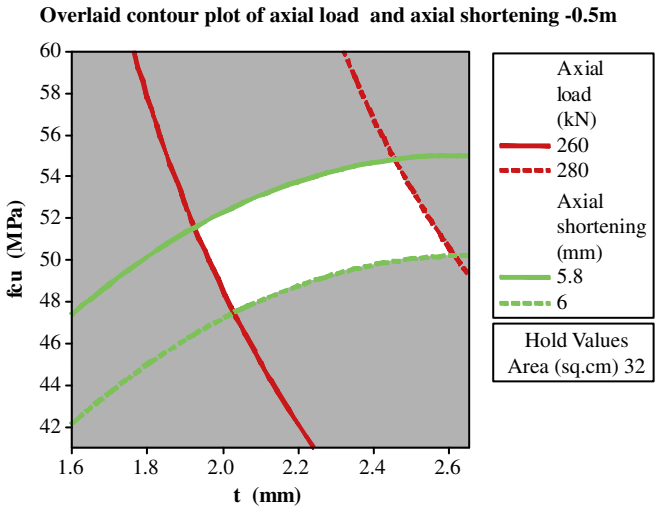

Fig. 18. Overlaid contour plot of axial load and axial shortening at ultimate point for CFTs – 0.5 m long (A = 3200 mm^2).

Table 9
Comparison of experimental results with AISC–LRFD and EC4 design codes.

Notation	P_{ue}/P_{AISC}			P_{ue}/P_{EC4}		
	1 m	0.7 m	0.5 m	1 m	0.7 m	0.5 m
$A_1t_1M_{30}$	0.57	1.03	1.18	0.44	0.88	1.05
$A_1t_2M_{30}$	0.72	1.08	1.06	0.56	0.92	0.95
$A_1t_3M_{30}$	0.75	1.08	1.09	0.59	0.95	1.00
$A_1t_1M_{40}$	0.68	1.02	1.11	0.51	0.86	0.98
$A_1t_2M_{40}$	0.78	1.14	1.16	0.59	0.96	1.02
$A_1t_3M_{40}$	0.89	1.11	1.17	0.69	0.96	1.06
$A_1t_1M_{50}$	0.79	1.10	1.16	0.58	0.91	1.01
$A_1t_2M_{50}$	0.91	1.17	1.16	0.67	0.97	1.01
$A_1t_3M_{50}$	0.97	1.17	1.19	0.74	1.00	1.07
$A_2t_1M_{30}$	1.16	1.24	1.23	0.94	1.08	1.10
$A_2t_2M_{30}$	1.17	1.29	1.28	0.96	1.13	1.16
$A_2t_3M_{30}$	1.15	1.23	1.23	0.96	1.09	1.13
$A_2t_1M_{40}$	1.18	1.22	1.22	0.94	1.04	1.08
$A_2t_2M_{40}$	1.20	1.24	1.26	0.97	1.07	1.13
$A_2t_3M_{40}$	1.16	1.20	1.17	0.95	1.05	1.06
$A_2t_1M_{50}$	1.14	1.15	1.14	0.88	0.96	1.00
$A_2t_2M_{50}$	1.18	1.17	1.18	0.93	1.00	1.04
$A_2t_3M_{50}$	1.15	1.13	1.14	0.92	0.98	1.03
$A_3t_1M_{30}$	1.13	1.33	1.35	0.96	1.18	1.22
$A_3t_2M_{30}$	1.07	1.26	1.28	0.92	1.13	1.17
$A_3t_3M_{30}$	1.13	1.16	1.19	0.99	1.05	1.10
$A_3t_1M_{40}$	1.13	1.23	1.25	0.95	1.07	1.11
$A_3t_2M_{40}$	1.14	1.17	1.20	0.96	1.04	1.08
$A_3t_3M_{40}$	1.09	1.12	1.11	0.94	1.01	1.02
$A_3t_1M_{50}$	1.10	1.13	1.14	0.90	0.98	1.01
$A_3t_2M_{50}$	1.09	1.12	1.11	0.91	0.98	0.99
$A_3t_3M_{50}$	1.04	1.06	1.07	0.89	0.94	0.97
Mean	1.02	1.16	1.18	0.82	1.01	1.06
SD	0.18	0.08	0.07	0.17	0.08	0.07
COV	18.16	6.59	5.80	20.90	7.73	6.22

the Table 9. The comparisons of results indicate that, predicted ultimate load carrying capacity for 1 m length of CFTs from both the design codes is much higher as compared to experimental values. But for 0.5 m and 0.7 m, predictions of ultimate load by design codes are fairly good.

5. Conclusions

Results of experimental investigations on circular CFT samples with B/t ratio of 9.4–25 and L/D ratio of 6.25–20 have been presented in this paper. From the experimental results, following broad conclusions can be drawn:

1. Regression models developed with minimum number of experiments based on Taguchi method, predict the axial load carrying capacity very well and reasonably well for axial shortening at ultimate point.
2. Cross-sectional area of the steel tube has the most significant effect on both the ultimate axial load and corresponding axial shortening of the CFTs.
3. Regression models developed using Response Surface Method, for ultimate axial load and corresponding axial shortening, account the interaction between the test variables.
4. Larger variation between experimental values and predicted values from design codes, for slender CFTs indicates more studies are needed and refinement of codal provisions.

Acknowledgement

The authors are grateful to M/s Shankara Pipes Private Limited, Bangalore, India for providing all the steel tubes used in the experimental programme.

References

[1] Shams M, Saadeghvaziri MA. State of the art of concrete-filled steel tubular columns. ACI Struct J 1997;94(5):558–71.

[2] Liu Dalin, Gho Wie-Min, Yuan Jie. Ultimate capacity of high-strength rectangular concrete-filled steel hollow section stub columns. J Constr Steel Res 2003;59:1499–515.

[3] Elremaily Ahmed, Azizinamini Atorod. Behavior and strength of circular concrete-filled tube columns. J Constr Steel Res 2002;58: 1567–91.

[4] Tao Zhong, Han Lin-Hai, Wang Dong-Ye. Strength and ductility of stiffened thin-walled hollow steel structural stub columns filled with concrete. Thin Wall Struct 2008;46:1113–28.

[5] IS 10262-1982. Indian standard recommended guidelines for concrete mix design. Bureau of Indian Standards, New Delhi, India.

[6] Eurocode 4. Design of composite steel and concrete structures, part 1.1: general rules and rules for buildings. Commission of European Communities, British Standards Institution; 1994.

[7] Douglas montgomery, design and analysis of experiments. 5th ed. New York: John Wiley & Sons (ASIA) Pvt. Ltd.; 2004.

[8] Han L-H. Tests on stub columns of concrete-filled RHS sections. J Constr Steel Res 2002;58:353–72.

[9] Shakir-Khalil H, Zeghiche J. Experimental behavior of concrete filled rolled rectangular hollow section columns. J Struct Eng, ASCE 1989;67(19):346–53.

[10] Shakir-Khalil H, Mouli M. Further tests on concrete-filled rectangular hollow-section columns. J Struct Eng, ASCE 1990;68(20):405–13.

[11] Schneider SP. Axially loaded concrete-filled steel tubes. J Struct Eng, ASCE 1998;124(10):1125–38.

[12] American Institute of Steel Construction (AISC). Manual of steel construction: load and resistance factor design (LRFD), 2nd ed. Chicago; 1994.